GENERATION OF REALISTIC 2D TRANSVERSE MICROSTRUCTURES OF UNIDIRECTIONAL FIBRE-REINFORCED COMPOSITES USING A GENERATIVE ADVERSARIAL NETWORK

Rui Guo[1], Marco Alves[2], Mahoor Mehdikhani[1], Christian Breite[1], Yentl Swolfs[1]*

[1]Department of Materials Engineering, KU Leuven, Kasteelpark Arenberg 44 box 2450, 3001 Leuven, Belgium, rui.guo1@kuleuven.be
[2]Move.ai,14 Adeline Pl, London WC1B 3AJ, UK

Abstract: *Microstructure generators for unidirectional fibre-reinforced composites are a crucial step for the prediction and optimisation of their mechanical properties. The purpose of this study is to generate 2D realistic transverse microstructure of these composites using a deep convolutional generative adversarial network (DCGAN). To make detailed statistical comparisons between the real and synthetic microstructures in terms of the geometric characteristics, a fibre segmentation method based on the watershed segmentation was developed to separate each fibre. The results show a good agreement between the real and synthetic microstructures, which illustrate the capability and potential of the DCGAN to generate realistic transverse microstructures.*

Keywords: deep learning; microstructure generator; materials design; microstructural analysis; generative adversarial network

1. Introduction

Fibre-reinforced composites are used in a wide range of applications due to their excellent mechanical properties and low density [1]. To assess the effect of microstructural variability on their mechanical properties, the industry largely relies on experimental characterisation. This approach hampers the adoption of new material combinations and production processes. To overcome this issue, advanced virtual characterisation techniques are needed to bridge the relevant scales starting from the microscale.

Models that start at the microscale often need a reliable method to generate random fibre packings. Pyrz et al. [2] proposed a hard core method to simulate the actual random fibre packings, however, this method cannot generate packings with fibre volume fractions greater than 50% [3]. To address this limitation, more advanced algorithms have been proposed. Melro et al. [3] proposed a stirring method that can effectively overcome the jamming limit problem for fibre-reinforced composites and the fibre volume fraction can even marginally exceed 65%. Yang et al. [4] proposed a random sequential expansion algorithm that can generate microstructure with fibre volume fraction up to 68% when fibres are allowed to contact each other. However, these algorithms only consider the stochastic placement of the fibre. In real microstructures, resin-rich areas exist [5], which have important effects on the mechanical properties [5,6]. Therefore, algorithms, which can fully capture real microstructural features, like non-circular fibres, resin-rich areas, and diameter variations, are in ongoing research.

Due to the availability of copious amounts of image data, deep learning methods have become popular to create representations of material microstructures. Compared to traditional generation methods, methods based on the generative adversarial networks (GAN) do not have

 ©2022 1st Author et al. https://doi.org/ 10.5075/978-X-XXX-XXXXX-X published under CC BY-NC 4.0 license

assumptions of the features and patterns represented in the image data. Therefore, such models can learn the underlying data distribution from their input dataset directly and can generate large datasets of unique realistic microstructures, which follow the same characteristics. Currently, GANs have been applied for microstructural generation of porous media [7] [8] and energy materials [9][10], resulting in microstructures representative of the real ones.

In this work, we use a Deep Convolutional Generative Adversarial Network (DCGAN) [11] to generate realistic 2D representations of transverse microstructures of unidirectional fibre-reinforced composites. A fibre segmentation method was built based on the watershed. Detailed statistical methods were employed to compare the synthetic microstructures with the real microstructures in terms of the fibres' geometric characteristics.

2. Materials and method

2.1 Experimental microstructures

The material used was a thin-ply carbon fibre/epoxy prepreg consisting of GRAFIL 34-700WD-24 K-1.4%A carbon fibres (Mitsubishi, Japan) and a proprietary 736LT resin (North Thin Ply Technology, Switzerland). Specimens were produced by stacking multiple plies on top of each other and curing them using a computerised autoclave at KU Leuven, as previously described in [12]. The specimens were water-jetted to the desired cross-section and scanned at the ID19 beamline of the ESRF synchrotron. Imaging settings were chosen to ensure high-contrast and high-resolution reconstructed images. For the here used data, the CT projections were acquired using a mono-chromatic beam at 20 keV paired with a 10x optical magnification lens and the pco.edge 5.5 camera available at ID19. This resulted in a final voxel size of 0.65 µm. The raw data was cropped to focus on the centre region of the reconstructed CT image. The input dataset became thereby a volume of 1100 x 550 x 1800 pixel^3, which corresponds to 715 x 357.5 x 1170 µm^3.). A sample image for a transverse slice of the CT volume is shown in Fig. 1. The images show the non-uniform distribution of the fibre due to the layered structure of the thin plies. Especially on the ply boundaries, some resin-rich areas are captured.

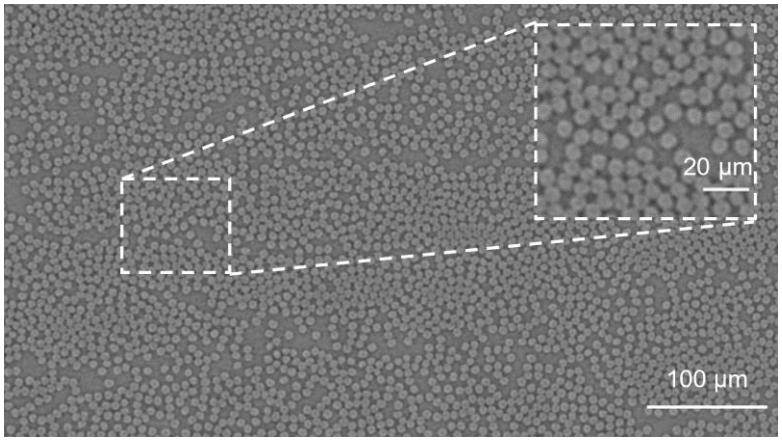

Fig. 1. A sample image for a transverse slice of the CT volume showing the cross-section of carbon fibres in an epoxy matrix

 ©2022 1st Author et al. https://doi.org/ 10.5075/978-X-XXX-XXXXX-X published under CC BY-NC 4.0 license

2.2 DCGAN implementation

Goodfellow et al. [13] first proposed the GAN. These networks are used to implicitly learn the probability distribution of a given data and then generate data with a similar probability distribution.

DCGAN can generate good results on small-sized images by introducing the convolutional neural networks [11]. Therefore, the large-sized input images were further cropped to the final 41.6 x 41.6 μm^2 (64 x 64 $pixel^2$) images. To obtain a sufficiently large training dataset, sampling of the cropped images with overlap was performed with a stride of 8 pixels as proposed in [9]. In addition, data augmentation methods were applied [14]. In total, 32390 images were obtained to train the DCGAN.

Table 1. summarises the specific networks and hyperparameters used for the DCGAN. The slope for all Leaky ReLU activations was 0.2, and batch normalisation was applied before the activation function. In the training process, the Adam optimum and a classic non-saturating GAN loss function [13] were used. The parameter $from_logits$ in this loss function was set as True. The learning rates for discriminator and generator were both 0.0002 and the momentum constants were $\beta_1 = 0.5, \beta_2 = 0.99$. The batch size was set to 64.

Table 1. The architecture of the DCGAN model for 2D transverse microstructures of unidirectional fibre-reinforced composite

Layer	Operations	Output	Kernel	Stride	Padding	Batch	Activation
	Input shape	(1*1*128)	-	-		-	-
G_1	Conv2DTranspose	(4*4*512)	4	1	Valid	Yes	ReLU
G_2	Conv2DTranspose	(8*8*256)	4	2	Same	Yes	ReLU
G_3	Conv2DTranspose	(16*16*128)	4	2	Same	Yes	ReLU
G_4	Conv2DTranspose	(32*32*64)	4	2	Same	Yes	ReLU
G_5	Conv2DTranspose	(64*64*1)	4	2	Same	No	Tanh
	Input shape	(64*64*1)	-	-		-	-
D_1	Conv2D	(32*32*64)	4	2	Same	No	LeakyReLU
D_2	Conv2D	(16*16*128)	4	2	Same	Yes	LeakyReLU
D_3	Conv2D	(8*8*256)	4	2	Same	Yes	LeakyReLU
D_4	Conv2D	(4*4*512)	4	2	Same	Yes	LeakyReLU
D_5	Conv2D	(1*1*1)	4	1	Valid	No	No

DCGAN was trained on a workstation based on the TensorFlow framework with a high-performance GPU (Nvidia RTX A5000). The training took around 16 minutes (25300 iterations).

 ©2022 1st Author et al. https://doi.org/ 10.5075/978-X-XXX-XXXXX-X published under CC BY-NC 4.0 license

After training, we were able to generate 100 microstructures in a few seconds only using the CPU.

2.3 Segmentation

To perform a statistical analysis of real and synthetic microstructures, an image-based fibre segmentation was implemented in MATLAB R2020b. The main steps are:

1. A Gaussian filter with a 2-D Gaussian smoothing kernel with standard deviation of 0.5 was used to remove the noise and smoothen the images. The Otsu threshold method was applied to automatically select a global threshold for converting grayscale images to binary images (see Fig. 2b).
2. A morphological opening operation with a disk-shaped kernel of radius 4 was used to remove artefacts (see Fig. 2c). It is worth noting that if the radius of the disk-shaped kernel is small, artefacts cannot be removed and if the kernel radius is too large, some fibres can be mistakenly removed as noise.
3. The image was eroded with the same disk kernel size as in step 2 first and then the Euclidean distance transformation was applied. After this, watershed ridge lines were found by using the watershed transformation. Based on these watershed ridge lines, most touching fibres were separated effectively. (See Fig. 2d).

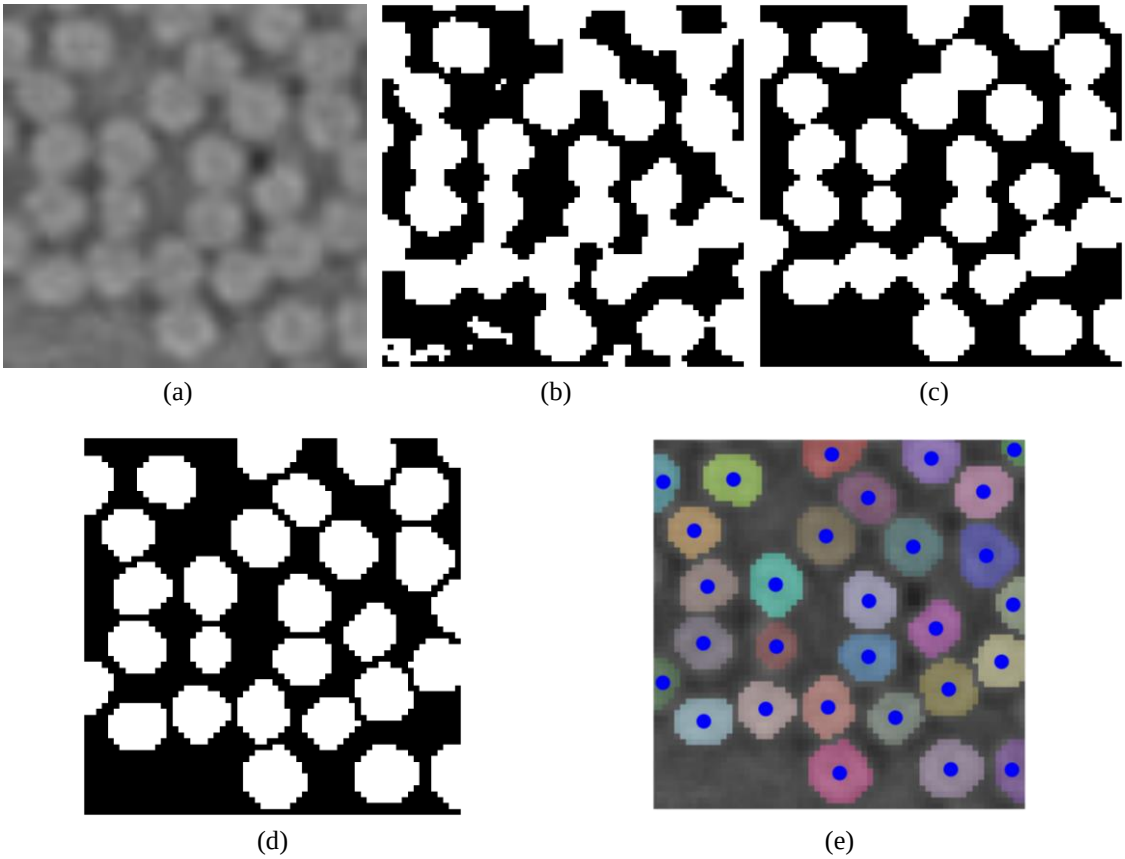

Fig. 2. Fibre segmentation methods based on watershed: (a) grayscale images, (b) binary images with some noises, (c) binary images after removing the noise, (d) binary image after separating the touching fibres, (e) overlay of the grayscale images and individual fibres

 ©2022 1st Author et al. https://doi.org/ 10.5075/978-X-XXX-XXXXX-X published under CC BY-NC 4.0 license

Fig. 2e shows the overlay of a binary sample image and the corresponding grayscale image. Each individual fibre is represented by a different colour. The blue points indicate the centre of each fibre, which were extracted according to the image moment method. These two functions and all further statistical analyses were implemented in Python code.

3. Results

3.1 Visual similarity

In contrast to the microstructures of porous media and energy materials, which are interconnected and irregular in shape, the fibres in the unidirectional fibre-reinforced composite studied have close to an ideal circular shape and there are no overlapping regions between the fibres. In addition, resin-rich areas and fibre clusters (densely packed fibres) exist in the real microstructure (see Fig. 3a). Nine randomly picked the synthetic microstructures were given in Fig. 3b. The synthetic microstructures visually capture the complex patterns in the real experimental data well. However, upon careful examination, a few unrealistic fibres can be detected, as is highlighted in Fig. 3b.

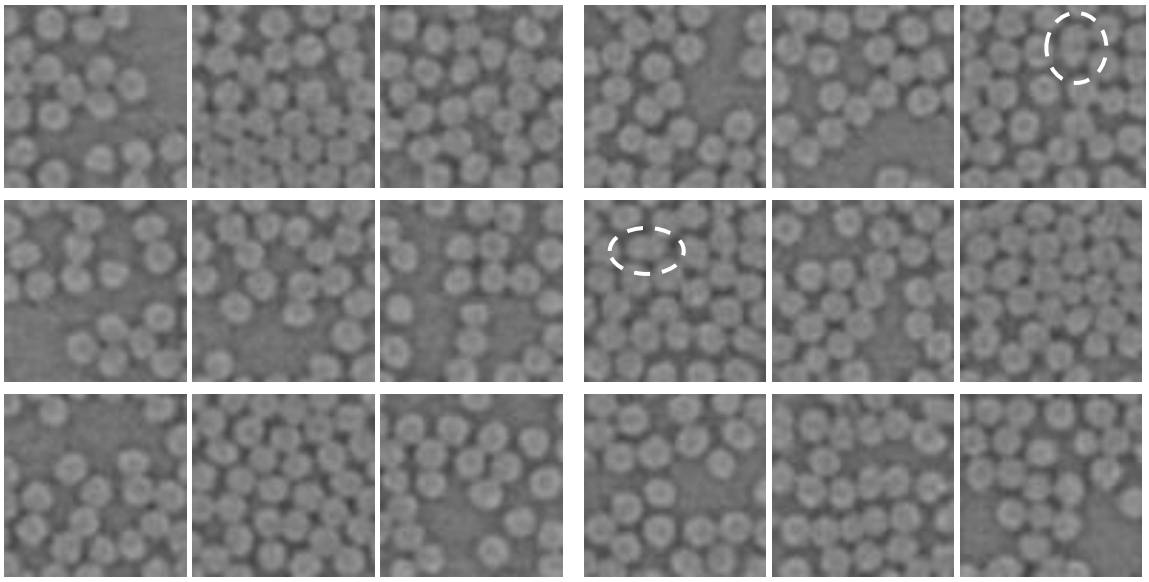

(a) (b)

Fig. 3. Comparison of samples of (a) real and (b) DCGAN-synthetic microstructures.

3.2 Statistical analysis

It is known that mechanical properties are affected by microstructural parameters, such as amongst others the fibre volume fraction, fibre diameter and clustering of fibres. All of these are captured in the synthetic images. To assess how well the synthetic data represents reality, a sample of 120 synthetic images generated by DCGAN was compared with 120 real images. The real images are unique without using any overlap and data augmentation to crop them from the input data.

The diameter of the same fibres type and even produced in the same batch by the manufacturer as the ones cured into composite and imaged using CT (our input data) was measured using a laser diffraction system (LDS) in [15]. The mean value and standard deviation of diameters for 89 fibres are 6.52 μm, 0.45, respectively. We assume the measurements using the LDS to be

 ©2022 1st Author et al. https://doi.org/ 10.5075/978-X-XXX-XXXXX-X published under CC BY-NC 4.0 license

precise and the ground truth for the following comparisons. 2050 fibres were extracted from the real images (64*64 pixel^2) after removing the fibres at the borders. The fibres at the image borders have to be excluded as their cross-section is often only partly included in the cropped CT image. The mean equivalent diameter for these fibres measured after segmentation is 6.25 µm with a standard deviation of 0.50, using Eq. (1), where f is equal to 1. Comparing to the LDS measurement value, this underestimated mean value is most likely due to the still low resolution of the images [16]. Assuming that the ground truth value should be obtained from the CT image if this limitation would be overcome, the actual fibre diameter can be reasonably obtained by applying an empirical factor f, as in Eq. (1), on the single fibre area. This factor is the ratio of the square of the average of the fibre diameters measured with LDS and the CT image measurements. It is around 1.088 for the current case.

$$D_{sing_fibre} = \sqrt{\frac{4 * S_{single_fibre} * f}{\pi}} * unit \tag{1}$$

Where D_{sing_fibre} is the equivalent diameter of a single fibre. S_{single_fibre} is the sum of the number of pixels in the fibre with pixel value equal to 255 in the binary images. f is the empirical factor considering the effect of the low-resolution images, and it is equal to 1 if no modifications is used on the fibres area. $unit$ is equal to the 0.65 µm.

For the 120 synthetic images, 1970 fibres were extracted. Some unrealistic fibres with equivalent diameters less than 4 µm and larger than 8 µm were found in the synthetic images. These unrealistic fibres accounted for about 1.4% of the fibres (=28 fibres) and thus were removed. Fig. 4a plots the histogram of the equivalent fibre diameter in both the real and synthetic images, and confirm the similarity of the distributions.

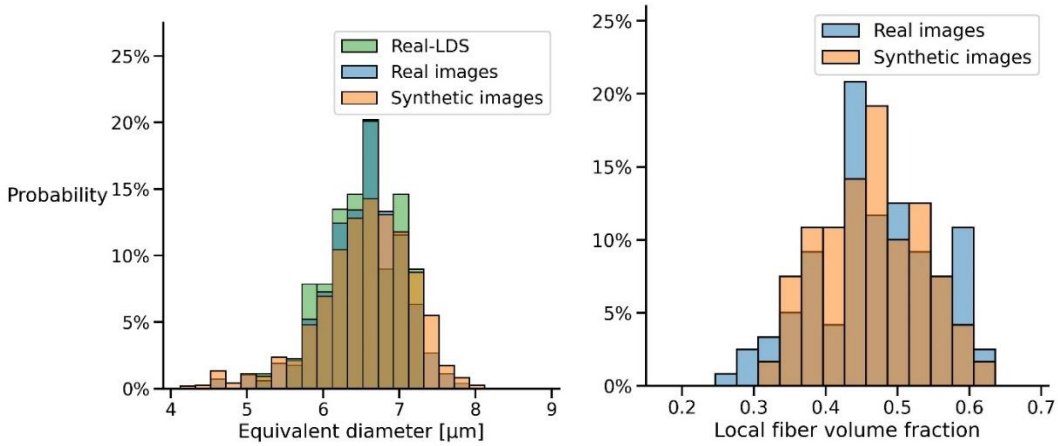

(a) (b)

Fig. 4. The histogram of the (a) equivalent diameter after removal of 28 unrealistic fibres for synthetic images and (b) local fibre volume fractions

After establishing the empirical factor f, the local fibre volume fraction was calculated using the Eq. (2) for sub-images of 1100 x 550 pixel^2. The mean value of the real images is varying from 43.1% to 46.9% after applying the empirical factor. This means the accuracy of resolving the correct equivalent fibre diameter has a significant effect on the local fibre volume fraction. Inspection of Fig. 4b confirms the similarity of the distributions of the local fibre volume fractions for the real and synthetic microstructures.

 ©2022 1st Author et al. https://doi.org/ 10.5075/978-X-XXX-XXXXX-X published under CC BY-NC 4.0 license

$$V_f = \frac{S_{all_fibres} * f}{S_{all_pixels}} \quad (2)$$

Where S_{all_fibres} is the sum of the number of pixels belonging to all fibres with pixel value equal to 255, and S_{all_pixels} is the sum of the number of all pixels, which is also equal to the image size.

4. Conclusions

We implemented a DCGAN model to generate realistic 2D transverse microstructures of unidirectional fibre-reinforced composites. The synthetic microstructures were verified versus the real microstructure in term of visual appearance and fibre statistical characteristics. This is a necessary step for the application of GAN-synthetic microstructures in future studies. Future work will expand this generator to 3D and will automate the creation of finite element models based on the synthetic images.

5. Acknowledgements

For provision of the synchrotron CT data, we kindly acknowledge I. Sinclair, M. N. Mavrogordato and E. Schöberl from University of Southampton µ-VIS lab. The related synchrotron experiment was conducted at ESRF ID19 with the help of L. Helfen. R. Guo would like to acknowledge his PhD scholarship from China Scholarship Council (202006430010). M. Mehdikhani would like to acknowledge his FWO Postdoc Fellowship, project ToughImage (1263421N). C. Breite would like to acknowledge FWO for the funding of his Postdoctoral Fellowship project COCOMI (1231322N).

6. References

[1] Biswal A, Swain SK. Smart composite materials for civil engineering applications. Elsevier Ltd; 2020. https://doi.org/10.1016/b978-0-08-103013-4.00011-x.

[2] Pyrz R. Quantitative description of the microstructure of composites. Part I: Morphology of unidirectional composite systems. Compos Sci Technol 1994;50:197–208. https://doi.org/10.1016/0266-3538(94)90141-4.

[3] Melro AR, Camanho PP, Pinho ST. Generation of random distribution of fibres in long-fibre reinforced composites. Compos Sci Technol 2008;68:2092–102. https://doi.org/10.1016/j.compscitech.2008.03.013.

[4] Yang L, Yan Y, Ran Z, Liu Y. A new method for generating random fibre distributions for fibre reinforced composites. Compos Sci Technol 2013;76:14–20. https://doi.org/10.1016/j.compscitech.2012.12.001.

[5] Huang F, Pang X, Zhu F, Zhang S, Fan Z, Chen X. Transverse mechanical properties of unidirectional FRP including resin-rich areas. Comput Mater Sci 2021;198:110701. https://doi.org/10.1016/j.commatsci.2021.110701.

[6] Sharifpour F, Montesano J, Talreja R. Micromechanical assessment of local failure mechanisms and early-stage ply crack formation in cross-ply laminates. Compos Sci Technol 2022;220:109286. https://doi.org/10.1016/j.compscitech.2022.109286.

[7] Mosser L, Dubrule O, Blunt MJ. Stochastic reconstruction of an oolitic limestone by generative adversarial networks 2017:1–22.

[8] Mosser L, Dubrule O, Blunt MJ. Reconstruction of three-dimensional porous media using generative adversarial neural networks. Phys Rev E 2017;96. https://doi.org/10.1103/PhysRevE.96.043309.

 ©2022 1st Author et al. https://doi.org/ 10.5075/978-X-XXX-XXXXX-X published under CC BY-NC 4.0 license

[9] Gayon-Lombardo A, Mosser L, Brandon NP, Cooper SJ. Pores for thought: generative adversarial networks for stochastic reconstruction of 3D multi-phase electrode microstructures with periodic boundaries. Npj Comput Mater 2020;6:1–11. https://doi.org/10.1038/s41524-020-0340-7.

[10] Hsu T, Epting WK, Kim H, Abernathy HW, Hackett GA, Rollett AD, et al. Microstructure Generation via Generative Adversarial Network for Heterogeneous, Topologically Complex 3D Materials. Jom 2021;73:90–102. https://doi.org/10.1007/s11837-020-04484-y.

[11] Radford A, Metz L, Chintala S. Unsupervised representation learning with deep convolutional generative adversarial networks. ICLR 2016:1–16.

[12] Breite C, Gorbatikh L, Lomov S V, Swolfs Y. Automated image analysis of ultrafast synchrotron CT scans to experimentally characterize the fibre break development during in-situ tensile tests. ICCM22 22nd Int Conf Compos Mater Melb 2019.

[13] Goodfellow I, Pouget-Abadie J, Mirza M, Xu B, Warde-Farley D, Ozair S, et al. Generative adversarial networks. NIPS 2014. https://doi.org/10.1145/3422622.

[14] Tran N, Tran V, Nguyen N, Nguyen T, Cheung N-M. On Data Augmentation for GAN Training. IEEE Trans Image Process 2021;30:1882–97.

[15] Mesquita F, Bucknell S, Leray Y, Lomov S V., Swolfs Y. Single carbon and glass fibre properties characterised using large data sets obtained through automated single fibre tensile testing. Compos Part A Appl Sci Manuf 2021;145:106389. https://doi.org/10.1016/j.compositesa.2021.106389.

[16] Emerson MJ, Dahl VA, Conradsen K, Mikkelsen LP, Dahl AB. Statistical validation of individual fibre segmentation from tomograms and microscopy. Compos Sci Technol 2018;160:208–15. https://doi.org/10.1016/j.compscitech.2018.03.027.

 ©2022 1st Author et al. https://doi.org/ 10.5075/978-X-XXX-XXXXX-X published under CC BY-NC 4.0 license